

RESEARCH ON FLIGHT DYNAMICS AND CONTROL CHARACTERISTICS OF MULTI-UAV WINGTIP-LINKED FLIGHT

Rui Wang[1,2], Yunheng Wu[1,2], Zhou Zhou[1,2], Sensen Yao[1,2], Ziyang Zhang[1,2]

[1]School of Aeronautics, Northwestern Polytechnical University, Xi'an, China
[2]National Key Laboratory of Aircraft Configuration Design, Xi'an, China.

Abstract

Wingtip-linked flight of multiple UAVs can substantially improve flight performance, yet these configurations exhibit dynamic behaviors distinctly different from conventional aircraft. This study focuses on flight dynamics and control for wingtip-linked multi-UAV assemblies. Systematic research is conducted on dynamic modeling, aerodynamic analysis, modal characteristics, control effectiveness and dynamic evolution laws, covering wingtip-linked UAV groups ranging from 1 to 7 units. A generalized theoretical framework applicable to arbitrary unit numbers, hinge stiffness and flight layouts is established and verified through flight tests.

Keywords: wingtip-linked UAVs, flight dynamics, Spatial Operator Algebra (SOA) Method, control efficiency, flight test

1. Introduction

1.1 Current Research Status

The demand for high-altitude, long-endurance (HALE) flight continuously drives the optimization of the aerodynamic and structural efficiency of aircraft. As a novel configuration that integrates the flexibility of small unmanned aerial vehicles (UAVs) and the endurance of HALE aircraft, the wingtip-linked compound multi-body aircraft has demonstrated significant application potential.

Regarding research on compound multi-body aircraft flight, McGill et al. [1] analyzed the aerodynamics and aerodynamic control during the wingtip-linking process through extensive wind tunnel tests, demonstrating that a compound aircraft with a wingtip-linked configuration consisting of an F-84 fighter and a transport aircraft can realize aerodynamic lift benefits of 20% to 40%.

Montalvo [2] put forward the concept of "meta aircraft" and analyzed the corresponding flight dynamics in wingtip-to-wingtip and tip-to-tail configurations, together with an analysis of the number of linked UAV units. The controllability [3] and connection control laws [4] of the compound aircraft were investigated as well. Finally, Montalvo linked two identical aircraft [5] and conducted a flight test using a feedback control law that included both take-off and landing.

Cooper [6] designed an easily assembled compound multi-body aircraft, performed simulation analysis on the wingtip linking process adapting a leader-follower guidance algorithm, and simulated the linking process of three aircraft by designing an outer-loop trajectory control law and an inner-loop attitude control law. Cooper also studied the flight performance of the compound aircraft from the perspective of aerodynamics, designed a prototype, and conducted level flight tests along with aerial separation tests of the UAV unit.

From a conceptual design perspective, Alexander Köthe [7] presented a conceptual design scheme for a wingtip-linked aircraft. For further investigation, they developed a flight path controller and

carried out experiments. Alexander also performed linearization and modal analysis on the aircraft, adapted control allocation and eigenstructure assignment [8][9] to design an inner-loop control law for the deformation motion of the multi-body aircraft, and subsequently designed a trajectory controller to complete a full-process simulation [10].

Based on Montalvo's research, An Chao et al. [11] conducted dynamic modeling and studied the wingtip linking performance of a two-unit hinged compound aircraft. They designed a PID control law and completed flight tests of a prototype with three UAV units linked by wingtip hinges.

However, the innovative configuration of multi-aircraft collaborative flight introduces a series of core technical challenges. The strong aerodynamic coupling among multiple UAV unit and the additional degrees of freedom introduced by the hinge connections render the dynamic modeling methods for traditional single aircraft inapplicable. Dynamic changes in parameters such as the number of UAV unit, hinge stiffness, and trim configurations result in highly complex dynamic characteristics and inherent instability within the system.

Köthe et al. [12] studied the dynamics of multi-body high-altitude aircraft using the Kane method and potential flow theory (vortex lattice method); their results pointed out that the stiffness and location of the joint between both wingtips is a key factor in the flight mechanics of linked aircraft. They transferred the dynamics of a highly flexible multi-body aircraft into those of a classical rigid-body aircraft by adapting control allocation and eigenstructure assignment.

Yang et al. [13] conducted numerical simulation and stability analysis on compound multi-body aircraft consisting of two and three UAV units linked by wingtips. They proved the inherent instability of the compound aircraft through modal analysis and proposed a feedback controller to eliminate this instability.

Zhu Entong et al. [14] established the flight dynamics model of a three-unit compound aircraft based on Lagrange equations in terms of quasi-coordinates. They studied the mechanism by which the roll degree of freedom introduced by the hinge connection significantly impacts the rigid-body modes of the vehicle, analytically derived the modal coupling mechanisms and evolution laws, and verified them through flight experiments.

Y. Fan et al. [15] researched a highly flexible morphing aircraft composed of three UAV units linked via wingtip hinges and proposed a controller structure based on NDI and NESO methods, which has the ability to change the dynamic characteristics of the multi-body aircraft by controlling the structural shape of the wings. Hao L. et al. [16] proposed a modified Kalman particle swarm optimization algorithm for highly flexible morphing aircraft with multiple control surfaces to maximize the attainable moment subset. Simulation results showed that a trade-off exists between flight performance and control performance in highly flexible morphing aircraft.

1.2 Contributions of this Paper

Currently, research on the flight dynamics of wingtip-linked compound aircraft has mainly focused on combinations of three or fewer UAV units. Compared to a single aircraft, a three-unit combination introduces only two extra relative roll degrees of freedom. However, as the number of UAVs increases further, the degrees of freedom surge rapidly, significantly increasing the order and computational complexity of the dynamic equations. There is a lack of generalized modeling frameworks suitable for such high-dimensional systems. Furthermore, modal analyses in existing studies are limited to identifying a few modes in three-unit combinations. The evolution laws and dominant factors of the numerous symmetric/anti-symmetric flapping modes derived from the high-dimensional motion of larger compound aircraft remain insufficiently clear in academia. Existing modal definitions and nomenclatures fail to cover the new modal types present in multi-unit combinations, resulting in a lack of standardized criteria for dynamic characteristic analysis.

Therefore, developing a generalized method for describing the deformation patterns and flight characteristics of multi-UAV wingtip-linked combined flight can not only overcome the current limitations regarding the number of UAV units but also resolve the modeling, analysis, and control

challenges caused by multi-unit coupling. This yields profound theoretical innovation and practical engineering significance, offering critical technical support for advancing HALE aircraft toward larger-scale multi-body collaborative configurations.

This paper focuses on studying the multi-UAV wingtip-linked compound flight. Targeting the core characteristics of wingtip links and multi-body collaboration, systematic research is carried out on dynamic modeling, aerodynamic analysis, modal analysis, dynamic evolution laws, flight control, and engineering validation. A generalized theoretical framework applicable to an arbitrary number of UAV units, generalized spring stiffness, and arbitrary trim configurations is established, and its correctness is validated using flight test data.

The configuration design of the UAVs used for wingtip-linked compound flight is shown in Figure 1.



Figure 1 - Wingtip-linked compound multi-body aircraft

The UAV unit consists of a conventional-layout vehicle driven forward by a nose-mounted propeller thruster, with its thrust vector passing through the center of gravity. An elevator is used to control the pitch motion, ailerons (elevons) actuate the roll motion or provide high lift, and a rudder controls the yaw motion.

The main parameters of the UAV unit are shown in Table 1:

Table 1 - Main parameters of the UAV unit

General parameters		Inertial parameters	
Cruise Speed (m/s)	12.4	I_{xx} (kg·m^2)	0.05
Total Weight (kg)	1.45	I_{yy} (kg·m^2)	0.08
Reference Area (m^2)	0.32	I_{zz} (kg·m^2)	0.13
Reference Chord (m)	0.267	I_{xz} (kg·m^2)	0.003
Total Span (m)	1.24		

2. Dynamic Modeling

Dynamic modeling is the core foundation for revealing the flight characteristics of compound multi-body aircraft and supporting the design of control strategies. Compared to traditional single-body aircraft, compound multi-body aircraft achieve multi-unit coordinated flight through wingtip linking. This not only introduces additional degrees of freedom, such as relative roll between units, but also involves complex aerodynamic coupling and structural dynamic interactions, making it difficult for conventional modeling methods to accurately describe their dynamic behaviors. Therefore, conducting research on the dynamic modeling of wingtip-linked UAVs is the essential prerequisite for subsequent analysis of dynamic and control characteristics.

The Spatial Operator Algebra (SOA) method is a highly efficient dynamic modeling approach for multi-body systems with a computational efficiency of O(n). Due to its concise concepts, convenient derivation, and excellent computational accuracy, it has been widely applied in the dynamic modeling of large, complex, multi-degree-of-freedom multi-body systems (e.g., multi-arm spacecraft).

The core advantage of the SOA method lies in its ability to clearly describe the transmission and transformation of real physical quantities—such as forces, velocities, and accelerations—between

adjacent units in a multi-body system. Its computational efficiency and accuracy fully meet the engineering requirements for real-time dynamic simulation and control system design of compound multi-body aircraft. Therefore, this paper introduces the SOA method to construct a multi-body dynamic model tailored to the topological structure and coupling characteristics of compound multi-body aircraft, providing reliable support for subsequent characteristic analysis and control design.

However, this method has not yet been widely promoted in the field of multi-body aircraft modeling. On one hand, most traditional aircraft have fixed configurations and low complexity, thus lacking an urgent need for highly efficient modeling methods. On the other hand, during the flight of compound multi-body aircraft, strong aerodynamic coupling effects exist in the flow fields of the individual units. The combination rules and application forms of aerodynamic forces are not yet fully clarified, posing challenges to the application of the SOA method.

2.1 Spatial Operator Algebra Description of Aircraft Physical Quantities

The geometric relationship of the wingtip-linked multi-UAV assembly is shown in Figure 2, which simplifies it into a multi-rigid-body model composed of n UAV units. The wingtip linkages between adjacent UAV units are constrained by revolute hinges. During model establishment, the dimensions and clearances of the hinges are ignored. A vertical earth-fixed coordinate system $O_e x_e y_e z_e$ is established according to the right-hand rule. The center of mass of UAV unit *k* is selected as the origin to establish the body-fixed coordinate system $O_k x_k y_k z_k$, which moves together with the body of the multi-body aircraft.

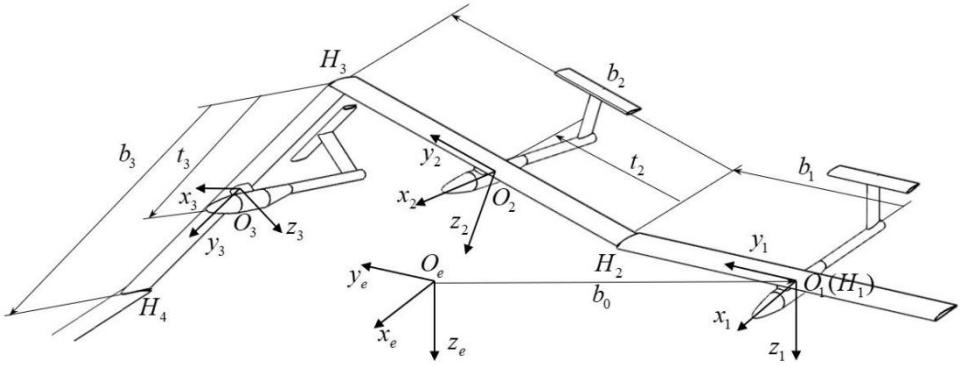


Figure 2 - Schematic diagram of multi-aircraft linkages

The translational and rotational physical quantities of each UAV unit *k* under the particle reference are expressed in the form of spatial vectors in Spatial Operator Algebra (SOA). The spatial velocity V_{bk}, spatial acceleration $\dot{V}_{bk}$, and spatial external force F_{bk} under the particle system are defined as follows:

$$V_{bk} = \begin{bmatrix} v_k \\ w_k \end{bmatrix}, \quad \dot{V}_{bk} = \begin{bmatrix} \dot{v}_k \\ \dot{w}_k \end{bmatrix}, \quad F_{bk} = \begin{bmatrix} f_k \\ g_k \end{bmatrix} \tag{1}$$

Where V_k, w_k are the tri-axial velocity and angular velocity of the unit body axes, and f_k, g_k are the sum of aerodynamic forces, gravity, and thrust acting on the unit particle. The spatial inertia operator M_k, including mass and inertia, is defined as follows:

$$M_k = \begin{bmatrix} m_k E_{3\times3} & -m_k t_k \times E_{3\times3} \\ m_k t_k \times E_{3\times3} & I_k \end{bmatrix} \tag{2}$$

For the n-body system of the hinged compound multi-body aircraft, to conveniently describe the transmission of physical quantities between units and establish subsequent recursive equations, the hinge point between each unit and the previous unit is taken as the reference point. Unit 1 (the rightmost UAV unit in Figure 2) is considered to be linked to the ground at its center of mass using a

virtual hinge. Therefore, it is necessary to transfer the forces/moments applied by the body axes in flight dynamics to the hinge points, and transfer the calculated velocities/accelerations to the particles for ease of analysis. The spatial transfer operator ϕ_{bk} from the hinge point of each UAV unit to the particle is defined as:

$$\phi_{bk} = \begin{bmatrix} E_{3\times3} & -t_k \times E_{3\times3} \\ 0 & E_{3\times3} \end{bmatrix} \tag{3}$$

The spatial transfer operator describes the equivalent transfer of spatial vectors on a rigid body. For unit *k*, the relationship between its spatial vectors referenced at the hinge point, V_k, $\dot{V}_k$, F_k, and the spatial vectors referenced at the particle, V_{bk}, $\dot{V}_{bk}$, F_{bk}, can be expressed as:

$$V_{bk} = \phi_{bk} V_k, \quad \dot{V}_{bk} = \phi_{bk} \dot{V}_k, \quad F_k = \phi_{bk}^T F_{bk} \tag{4}$$

2.2 Multi-Body Dynamic Recursive Relations Between Adjacent Units

The transmission of physical quantities between units depends on the constraint characteristics of the hinges. To establish a parameterized hinge model, a hinge state transition operator H_k is defined to describe the transmission relationship of physical quantities between units. Its column dimension represents the number of degrees of freedom between the units. If the units are linked by a revolute hinge around the x-axis, then $H_k = [0,0,0,1,0,0]^T$, the position of the non-zero element in the operator indicates that there is a roll degree of freedom around the x-axis between the units.

According to the Newton-Euler principle, the forward recursive relationship for velocity and acceleration between UAV unit, expressed using spatial operators, is:

$$\begin{cases} V_k = \phi_{k,k-1} V_{k-1} + H_k \dot{\vartheta}_k & k = 2,3,\cdots,n \\ \dot{V}_k = \phi_{k,k-1} \dot{V}_{k-1} + H_k \ddot{\vartheta}_k + a_k \\ a_k = \dot{\phi}_{k,k-1} V_{k-1} + \dot{H}_k \dot{\vartheta}_k \end{cases} \tag{5}$$

Where $\phi_{k,k-1}$ is the spatial transfer operator from the reference point of unit k-1 to the reference point of unit k, with the transfer vector being b_{k-1}; ϑ_k is the generalized displacement, representing the angular or linear displacement around hinge k, related to the degrees of freedom of the hinge; a_k is the Coriolis acceleration caused by coordinate rotation.

To describe the transmission relationship of forces between units, based on the rigid-body dynamic equations of the UAV unit, we have:

$$M_k \cdot \dot{V}_k + \Omega_k \cdot M_k \cdot V_k = F_k + F_k^c - \phi_{k+1,k}^T F_{k+1}^c \tag{6}$$

Where Ω_k is the velocity operator of the centrifugal force:

$$\Omega_k = \begin{bmatrix} w\times E_{3\times3} & 0_{3\times3} \\ v\times E_{3\times3} & w\times E_{3\times3} \end{bmatrix} \tag{7}$$

Subsequently, the backward recursive relationship for the hinge transmission force F_k^c between adjacent units is established:

$$\begin{cases} F_k^c = \phi_{k+1,k}^T \cdot F_{k+1}^c - F_k + F_k^g & k = n-1, n-2, \cdots, 1 \\ F_k^g = M_k \cdot \dot{V}_k + \Omega_k \cdot M_k \cdot V_k \\ T_k = H_k^T \cdot F_k^c \end{cases} \tag{8}$$

Where T_k is the joint-driving external force.

Defining the total system velocity operator of the compound multi-body aircraft as $\vec{V} = V_1^T, V_2^T, \cdots V_n^T$, and representing vectors such as the system Coriolis acceleration operator $\bar{a}$, inertia force operator $\bar{F}_g$, and external force operator $\bar{F}$ in the same form, while defining the system hinge state transition operator $\bar{H} = diag[H_1, H_2, \cdots, H_n]$ and system inertia operator $\bar{M} = diag[M_1, M_2, \cdots, M_n]$, the system

dynamic equations can be expressed as:

$$\begin{cases} \hat{M}\ddot{\vartheta} = \bar{T} + \bar{H}^T\Phi^T(\bar{F} - \bar{F}_g) - \bar{H}^T\Phi^T\bar{M}\Phi a \\ \bar{V} = \Phi\bar{H}\dot{\vartheta} \\ \hat{M} = \bar{H}^T\Phi^T\bar{M}\Phi\bar{H} \end{cases} \tag{9}$$

Where $\hat{M}$ represents the system generalized mass matrix; Φ is the spatial transfer operator. For the single-chain topological configuration of the compound multi-body aircraft, its expression is:

$$\Phi = \begin{bmatrix} E & 0 & 0 & 0 \\ \phi_{2,1} & \ddots & 0 & 0 \\ \vdots & \cdots & E & 0 \\ \phi_{n,1} & \cdots & \phi_{n,n-1} & E \end{bmatrix} \tag{10}$$

The dynamic equations (9) expressed in the formula reveal the equivalent relationship between the analytical method of Lagrange equations and the recursive method of Newton-Euler. The system hinge state transition operator H cannot be inverted, and inverting the generalized inertia matrix can only be done algebraically, with a computational efficiency of $O(n^3)$, which consumes a large amount of computation time.

2.3 Multi-Body Aircraft Dynamics Solution and State-Space Equation Establishment

The articulated-body algorithm was first proposed by Featherstone. This algorithm introduces the articulated-body assumption for spatial forces at hinges, where the interaction force between hinges can be described as a linear relationship with spatial acceleration $\dot{V}_k$:

$$F_k^c = \Pi_k \cdot \dot{V}_k + z_k \tag{11}$$

Where Π_k is the articulated-body inertia operator, representing the influence of the system's spatial inertia on unit k; z_k is the articulated-body bias force, representing the influence of non-zero interaction forces between units on the k-th rigid body.

Establishing the flight dynamic equations of the compound multi-body aircraft is essentially solving the forward dynamics problem of a multi-rigid-body system, which requires determining the generalized velocities and displacements of the system based on the input of external forces. By combining the relevant equations (5) (8) and (11), the backward recursive formulas for Π_k and z_k are obtained:

$$\begin{cases} \Pi_k = \phi_k^T \cdot \Pi_{k+1} \cdot \phi_k + M_k - \phi_k^T \cdot \Pi_{k+1} \cdot H_{k+1} \cdot \left(H_{k+1}^T \cdot \Pi_{k+1} \cdot H_{k+1}\right)^{-1} \cdot H_{k+1}^T \cdot \Pi_{k+1} \cdot \phi_k \\ z_k = \phi_k^* \cdot \Pi_{k+1} \cdot H_{k+1} \cdot \left(H_{k+1}^T \cdot \Pi_{k+1} \cdot H_{k+1}\right)^{-1} \cdot \left[T_{k+1} - H_{k+1}^T \cdot \left(\Pi_{k+1} \cdot a_{k+1} + z_{k+1}\right)\right] \\ +\phi_k^* \cdot \left(\Pi_{k+1} \cdot a_{k+1} + z_{k+1}\right) + \Omega_k \cdot M_k \cdot V_k - F_k \end{cases} \tag{12}$$

As well as the forward recursive relationship for acceleration $\ddot{\vartheta}_k$:

$$\ddot{\vartheta}_{k+1} = \left(H_{k+1}^T \cdot \Pi_{k+1} \cdot H_{k+1}\right)^{-1} \left\{T_{k+1} - H_{k+1}^T \cdot \left[\Pi_{k+1} \cdot \left(\phi_k \cdot \dot{V}_k + a_{k+1}\right) + z_{k+1}\right]\right\} \tag{13}$$

This formula (13) represents the multi-body dynamic equations in recursive form, which essentially shares the same form as the equations (9). In the recursive formulation, the most complex part of the calculation is only the inversion of a 6×6 matrix, which significantly improves computational efficiency.

The above equations describe the relative kinematic characteristics of the compound multi-body aircraft, where the dimension of the equations is the sum of the dimensions of ϑ_k. Taking Unit 1 as the reference body, it is considered to be linked to the inertial coordinate system by a virtual hinge. For Unit 1, its variable $\ddot{\vartheta}_1$ represents the linear and angular accelerations in the inertial coordinate system. The UAV units are linked by revolute hinges with relative roll degrees of freedom, where ϕ_k

represents the relative roll angle of Unit k with respect to Unit k-1.

The flight dynamic parameters such as angle of attack, sideslip angle, and attitude angle of each UAV unit obtained through calculation can accurately and completely characterize the spatial motion configuration of each unit in the multi-body aircraft. By integrating the attitude equation set, a (9+2n)-dimensional flight dynamics state-space equation for the compound multi-body aircraft is constructed:

$$\dot{x} = f(x) \tag{14}$$

Where the state vector $x = [u_1, v_1, w_1, p_1, q_1, r_1, \varphi_1, \theta_1, \psi_1, \vartheta_2, \dot{\vartheta}_2, \cdots, \vartheta_n, \dot{\vartheta}_n]^T$ contains the velocity and angular velocity of the reference unit under its body axes, the flight attitude Euler angles, the relative roll angles between units, and the relative roll angular velocities.

3. Dynamic Characteristic Analysis

3.1 Aerodynamic Characteristics of Wingtip-Linked Compound UAVs

There are differences in the aerodynamic coefficients of the same flight unit between the independent flight state and the compound flight state. This discrepancy arises from the aerodynamic interference effects brought about by the compound flight mode. When multiple UAV units are linked via wingtip links and fly collaboratively, the linking of the wingtips significantly weakens or eliminates the wingtip vortex structures that originally existed during independent flight. The elimination of these wingtip vortices directly alters the airflow characteristics over the main wing, leading to a reconfiguration of the spanwise distribution of aerodynamic forces on the main wing and an increase in the effective aspect ratio. Therefore, compared to when they fly independently, the aerodynamic characteristics of each UAV unit in compound flight (including lift distribution and induced drag characteristics) undergo non-negligible changes.

The vortex lattice method is employed to calculate the main aerodynamic characteristics of wingtip-linked compound aircraft with varying numbers of UAV unit. When the relative roll angles of the UAVs are all 0 degrees, the calculation results are shown in Table 2:

Table 2 - Main aerodynamic characteristics of wingtip-linked compound UAVs with different numbers of units

Number of UAVs	$C_{L\alpha}$	$C_{m\alpha}$	C_{lp}	C_{lr}
1	4.442	-0.904	-0.374	0.105
2	5.282	-0.935	-0.513	0.145
3	6.178	-0.943	-0.663	0.187
4	6.300	-0.943	-0.678	0.192
5	6.425	-0.943	-0.693	0.196
6	6.502	-0.943	-0.703	0.198
7	6.525	-0.943	-0.705	0.199

As indicated by the table above, the $C_{L\alpha}$ of the 7-aircraft combination increases by 46% compared to a UAV unit, demonstrating that wingtip linking can effectively improve the aerodynamic efficiency of UAVs. Simultaneously, C_{lp} increases by 88% compared to a UAV unit; thus, it is foreseeable that the dynamic characteristics of the compound aircraft will also be significantly different from those of a UAV unit.

3.2 Flight Performance of Wingtip-Linked Compound Aircraft

The control objective is to maintain all UAV units in level flight. After linking the wingtips from 1 to 7 UAVs, the trim throttle is shown in the following figure:

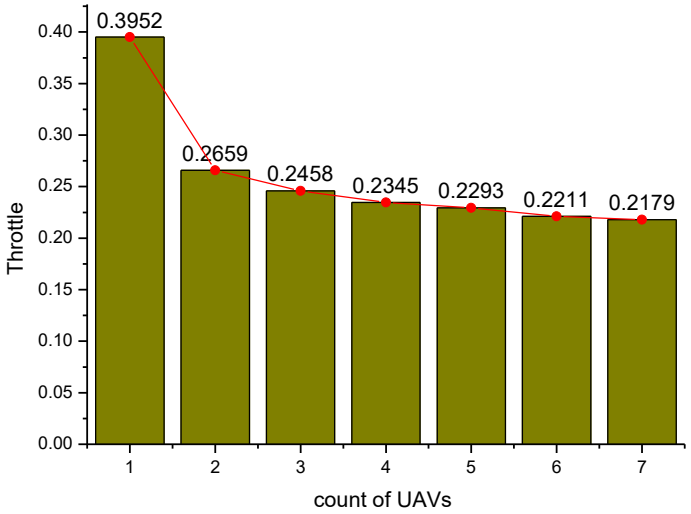


Figure 3 - Trim throttle variation curves for different numbers of linked units

Based on the trim throttle results ranging from one to seven aircraft, the throttle for seven aircraft is only 0.55 times that of a UAV unit. This indicates that the aspect ratio gain from the wingtip link combination substantially improves the lift-to-drag ratio, which is extremely beneficial for HALE flight.

3.3 Flight Stability of Wingtip-Linked Assemblies

Under the condition of rigid wingtip linkages for different numbers of UAV unit, the characteristic roots of the dynamic modes are shown below:

Table 3 - Characteristic root calculation results from single to seven aircraft

Mode	1 Unit	2 Unit	3 Unit	4 Unit	5 Unit	6 Unit	7 Unit
Short Period Mode	-10.7±6.4i	-11.0±7.7i	-11.0±7.5i	-11.1±7.7i	-11.4±7.7i	-11.3±7.6i	-11.3±7.6i
Phugoid Mode	-0.18±0.82i	-0.20±0.77i	-0.20±0.79i	-0.19±0.77i	-0.17±0.77i	-0.17±0.77i	-0.18±0.77i
Dutch Roll Mode	-2.15±7.66i	-0.94±3.03i	-0.78±1.94i	-0.68±1.46i	-0.66±1.16i	-0.64±0.96i	-0.63±0.84i
Roll Subsidence Mode	-13.9	-8.9	-7.3	-8.6	-9.0	-9.6	-9.76
Spiral Mode	0.209	0.186	0.1905	0.1496	0.1355	0.1234	0.1124
Symmetric Flapping Mode 1		-8.9±15.5i	-4.5±3.7i	-10.3±19.5i	-6.9±10.6i	-11.0±20.5i	-8.3±14.6i
Symmetric Flapping Mode 2				-8.9	-8.2	-8.7	-9.2
Symmetric Flapping Mode 3 / Special Motion				-0.99	-0.48	-0.23	-0.13
Anti-Sym. Flapping Mode 1			-9.8±18.3i	-6.4±7.3i	-10.9±20.1i	-7.7±12.9i	-11.11±20.9i
Anti-Sym. Flapping Mode 2					-4.7±2.4i	-5.5±5.4i	-6.1±7.7i
Anti-Sym. Flapping Mode 3						-6.8	-7.5
Anti-Sym. Flapping Mode 4						-1.7	-0.7
Symmetric Flapping Mode 4							-4.9±1.9i

As depicted in the table, with an increasing number of UAV unit in the compound assembly, the frequency and damping ratio of the short period mode show a slight upward trend; the frequency and damping of the Dutch roll mode gradually decrease; and the divergence rate of the spiral mode slows down. The characteristics of the flapping modes are correlated with the parity (odd/even nature) of the number of flight units, exhibiting differentiated evolution patterns. When the number of UAV unit

is ≥ 4, non-periodic special motion modes with unclear physical phenomena begin to appear, and the flight dynamics become increasingly complex.

In the configuration of seven UAVs with linked wingtips, the characteristic roots of the modes corresponding to different hinge stiffness k are shown in the following table:

Table 4 - Modal characteristic roots of seven-aircraft configuration

Mode	k=1	k=3	k=5	k=7
Short Period Mode	-11.40±7.67i	-11.41±7.68i	-11.40±7.68i	-11.40±7.68i
Phugoid Mode	-0.11±0.78i	-0.12±0.78i	-0.12±0.78i	-0.12±0.78i
Dutch Roll Mode	-0.54±0.81i	-0.52±0.82i	-0.52±0.82i	-0.52±0.81i
Roll Subsidence Mode	-10.16	-10.07	-9.96	-9.86
Spiral Mode	0.069	0.060	0.057	0.056
Symmetric Flapping Mode 1	-14.25, -2.43	-8.42±5.95i	-8.40±10.27i	-8.40±13.26i
Symmetric Flapping Mode 2	-8.20, -0.39	-7.68, -1.22	-7.07, -2.30	-4.84±0.31i
Symmetric Flapping Mode 3	-10.65	-10.13	-9.68	-9.35
Anti-Sym. Flapping Mode 1	-18.68, -7.70	-11.28±9.14i	-11.26±14.92i	-11.25±19.03i
Anti-Sym. Flapping Mode 2	-11.63, -1.04	-5.52±0.66i	-6.07±4.68i	-6.14±6.78i
Anti-Sym. Flapping Mode 3	-3.64	-9.03	-7.89	-7.66
Anti-Sym. Flapping Mode 4	-0.068	-0.24	-0.42	-0.62
Special Motion Mode	-0.048	-0.072	-0.096	-0.11

As the table illustrates, the hinge stiffness exerts a weak impact on the conventional modes (short period, phugoid, etc.) of the compound aircraft, yet it possesses a significant regulatory effect on the flapping modes and special modal characteristics. Increasing the hinge stiffness can transform most flapping modes from real roots to conjugate complex roots, simultaneously enhancing the modal oscillation frequency and damping characteristics. Among these, the sensitivity of the anti-symmetric flapping modes to stiffness variations is significantly higher than that of the symmetric flapping modes.

When the trim configuration of the compound aircraft changes, the variation in the relative roll angle exerts a regular influence on modal stability. The damping ratio of the short period mode improves with an increase in the roll angle, and the stability of the Dutch roll mode is simultaneously enhanced. The stability of the spiral mode is closely related to the configuration: it is in an unstable state under a dihedral configuration and its stability is significantly enhanced under an anhedral configuration. The damping coefficient and oscillation frequency of the flapping modes exhibit a significant regular evolution with changes in the relative roll angle.

3.4 Controllability of Wingtip-Linked Assemblies

When varying numbers of UAV unit are linked, the elevon deflections $C_{L\delta_a}$ on each UAV unit (with control surfaces on the left and right wings actuated separately) are shown in the following table:

Table 5 - Elevon $C_{L\delta a}$ for different numbers of linked UAVs

num	1l	1r	2l	2r	3l	3r	4l	4r	5l	5r	6l	6r	7l	7r
7	1.335	1.657	1.727	1.751	1.765	1.771	1.774	1.774	1.771	1.765	1.751	1.727	1.657	1.335
6	1.335	1.657	1.727	1.751	1.765	1.771	1.771	1.765	1.751	1.727	1.657	1.335		
5	1.330	1.649	1.717	1.739	1.748	1.748	1.739	1.717	1.649	1.330				
4	1.325	1.642	1.707	1.724	1.724	1.707	1.642	1.325						
3	1.317	1.627	1.683	1.683	1.627	1.317								
2	1.297	1.587	1.587	1.297										
1	1.217	1.217												

Based on the table above, the roll control effectiveness $C_{l\delta_a}$ of each elevon relative to the center point of the compound assembly can be calculated as follows:

Table 6 - Elevon $C_{l\delta a}$ for different numbers of linked UAVs

num	1l	1r	2l	2r	3l	3r	4l	4r	5l	5r	6l	6r	7l	7r
7	-0.620	-0.651	-0.555	-0.438	-0.315	-0.190	-0.063	0.063	0.190	0.315	0.438	0.555	0.651	0.620
6	-0.612	-0.621	-0.504	-0.365	-0.221	-0.074	0.074	0.221	0.365	0.504	0.621	0.612		

5	-0.599	-0.577	-0.429	-0.261	-0.087	0.087	0.261	0.429	0.577	0.599
4	-0.580	-0.513	-0.320	-0.108	0.108	0.320	0.513	0.580		
3	-0.549	-0.407	-0.140	0.140	0.407	0.549				
2	-0.486	-0.198	0.198	0.486						
1	-0.304	0.304								

As seen from the table above, after the wingtips of multiple UAVs are linked, the roll control derivative of the elevons doubles compared to that of a UAV unit due to the increased wingspan.

In practical applications, it is also necessary to consider that after wingtip linking, the moment of inertia of the compound aircraft will change. Because the dimensional derivative is directly proportional to the roll angular acceleration, it can intuitively evaluate the roll control effectiveness of the elevons. This derivative is defined as:

$$\bar{L}_{\delta_a} = C_{l\delta_a} q S_{com} b_{com} / I_{x,com} \tag{15}$$

Where: q is the flight dynamic pressure, S_{com} is the reference wing area of the assembly, b_{com} is the span of the assembly, and $I_{x,com}$ is the moment of inertia of the assembly around the x-axis.

For a compound multi-body aircraft, the parallel axis theorem can be employed to calculate $I_{x,com}$:

$$I_{x,com} = nI_x + \frac{mb^2 n(n^2-1)}{12} \tag{16}$$

Where: I_x is the moment of inertia of a UAV unit around the x-axis, and n is the number of UAV unit.

By substituting the corresponding data, the dimensional derivatives $\bar{L}_{\delta_a}$ for different combination quantities can be obtained as shown below:

Table 7 - Elevon $\bar{L}_{\delta_a}$ for different numbers of linked UAVs

num	1l	1r	2l	2r	3l	3r	4l	4r	5l	5r	6l	6r	7l	7r
7	-22.4	-23.5	-20.1	-15.8	-11.4	-6.9	-2.3	2.3	6.9	11.4	15.8	20.1	23.5	22.4
6	-25.9	-26.3	-21.3	-15.4	-9.3	-3.1	3.1	9.3	15.4	21.3	26.3	25.9		
5	-30.7	-29.6	-22.0	-13.4	-4.5	4.5	13.4	22.0	29.6	30.7				
4	-37.7	-33.4	-20.8	-7.0	7.0	20.8	33.4	37.7						
3	-49.3	-36.5	-12.6	12.6	36.5	49.3								
2	-72.8	-29.7	29.7	72.8										
1	-227.4	227.4												

As shown in the table above, the combined configuration of wingtip linking causes the moment of inertia for the UAV's roll degree of freedom to increase dramatically, so the roll control effectiveness of the assembly is reduced by half compared to a UAV unit, and the total effectiveness from 2 to 7 units does not change significantly.

Combining the previous flight stability analysis, the roll-flap motion degree of freedom of the compound aircraft is highly prone to divergence. It is desirable to have stronger roll control effectiveness for stability augmentation control, which imposes higher requirements on the flight control of the compound multi-body aircraft.

4. Flight Validation of Wingtip-Linked Compound Aircraft

4.1 Flight Validation with Different Hinge Stiffnesses

A three-unit compound configuration is selected as the validation object, and the experiment is conducted in two stages. In the first stage, the hinge stiffness is set to 0, and no configuration control input is applied, only maintaining the basic attitude stability of each UAV unit. In the second stage, rubber bands are added between the hinges of adjacent aircraft to introduce hinge stiffness (K is approximately 0.144 N·m/rad), and configuration control is added, while the remaining experimental conditions are kept consistent with the first stage.

When there is no hinge stiffness (K=0) and no configuration control input is applied, two typical modes—obvious symmetric flapping and anti-symmetric flapping—appear during the three-aircraft flight. During the symmetric flapping mode, the side units (aircraft 1 and 3) exhibit synchronized, in-phase rolling motions relative to the reference aircraft (aircraft 2). During the anti-symmetric flapping mode, the side UAV units roll in opposite directions with a phase difference of 180°, forming an alternating swinging phenomenon, which is basically consistent with the theoretical analysis results.

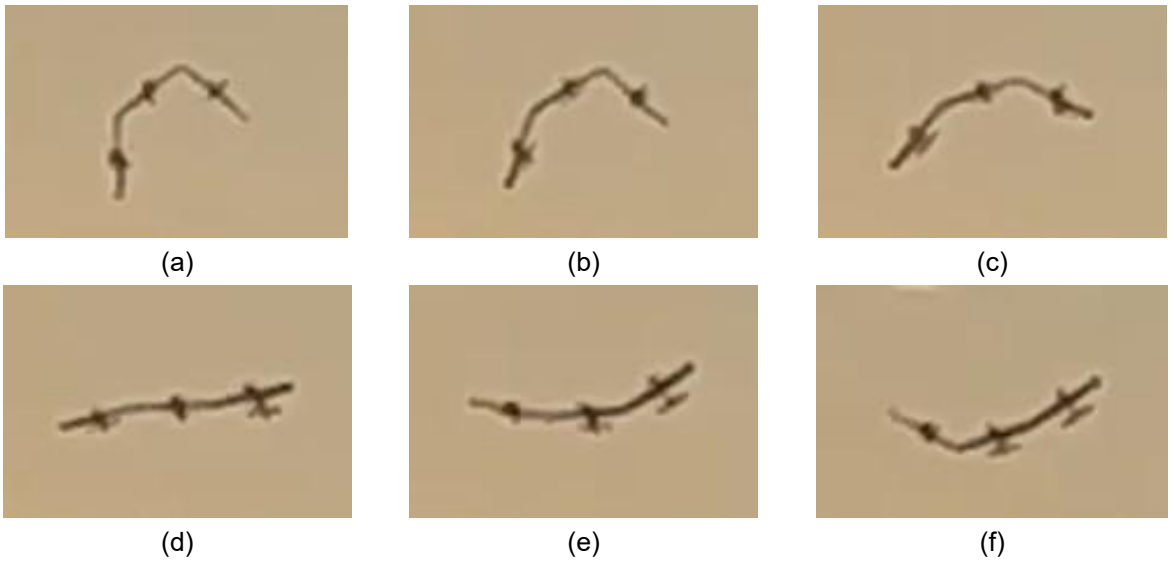


Figure 4 - Three-aircraft symmetric flapping mode

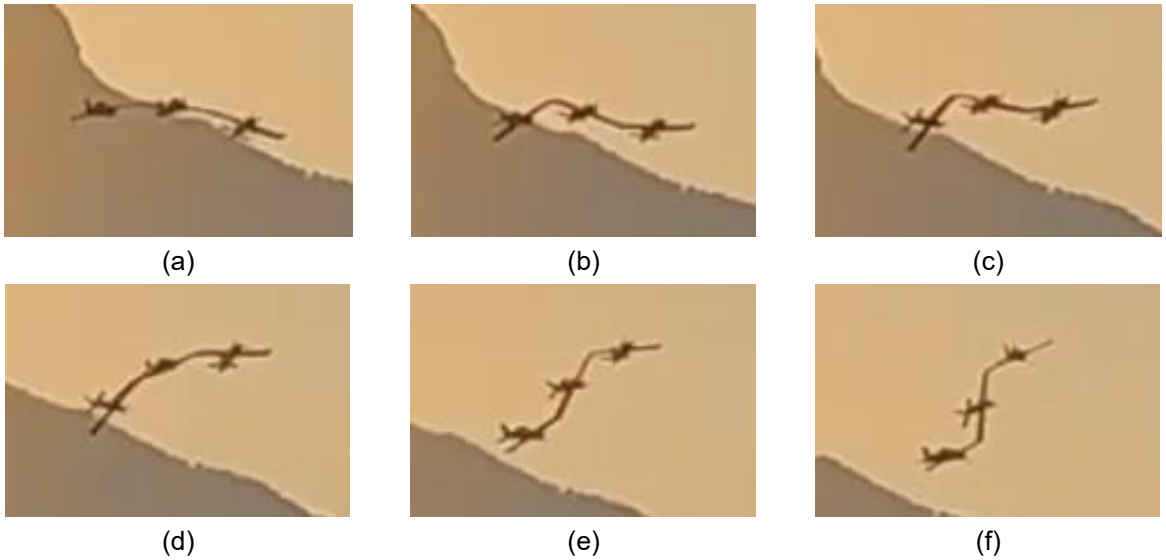
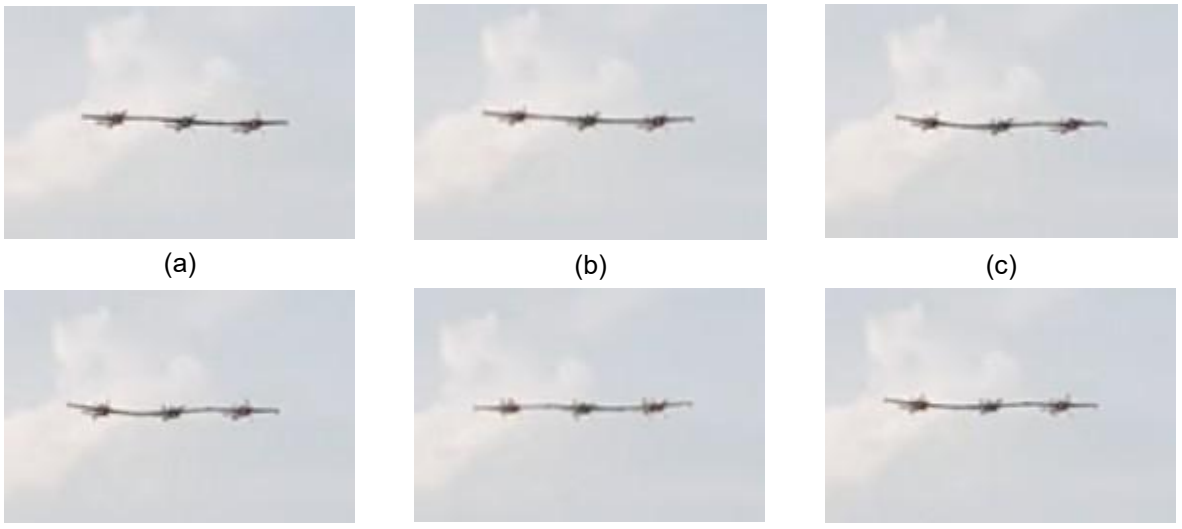


Figure 5 - Three-aircraft anti-symmetric flapping mode

Under the conditions of zero hinge stiffness and no configuration control, the symmetric and anti-symmetric flapping modes of the three aircraft are easily excited during flight. In actual flight, this manifests as a superposition of the two modes, resulting in an indescribable transformation of the compound aircraft's configuration. After adding rubber bands between adjacent aircraft to increase the hinge stiffness and implementing configuration control, the flapping modes of the three aircraft are effectively suppressed. The following figure shows an extremely subtle anti-symmetric flapping motion, where it can be seen that the flapping amplitude is significantly reduced compared to before, and the frequency has also decreased. This can partially verify the conclusion from the dynamic

characteristic analysis of compound multi-body aircraft with variable hinge stiffness in Chapter 3, which stated that increasing the equivalent spring stiffness significantly enhances the damping characteristics of the flapping motion.



(a) (b) (c)

(d) (e) (f)

Figure 6 - Subtle flapping after adding hinge stiffness and configuration control

4.2 Flight Validation of Different Trim Configurations

During the process of conducting multi-aircraft linked flight tests, there were multiple occurrences of flight mode divergence eventually leading to instability and crashing. Systematically observing these flight test results reveals a general pattern: whether it is the divergence process of a three-unit or five-UAV unit, it is always caused by the side UAV unit on one or both sides adopting an excessive dihedral angle, which gradually diverges and leads to the instability of the compound aircraft.

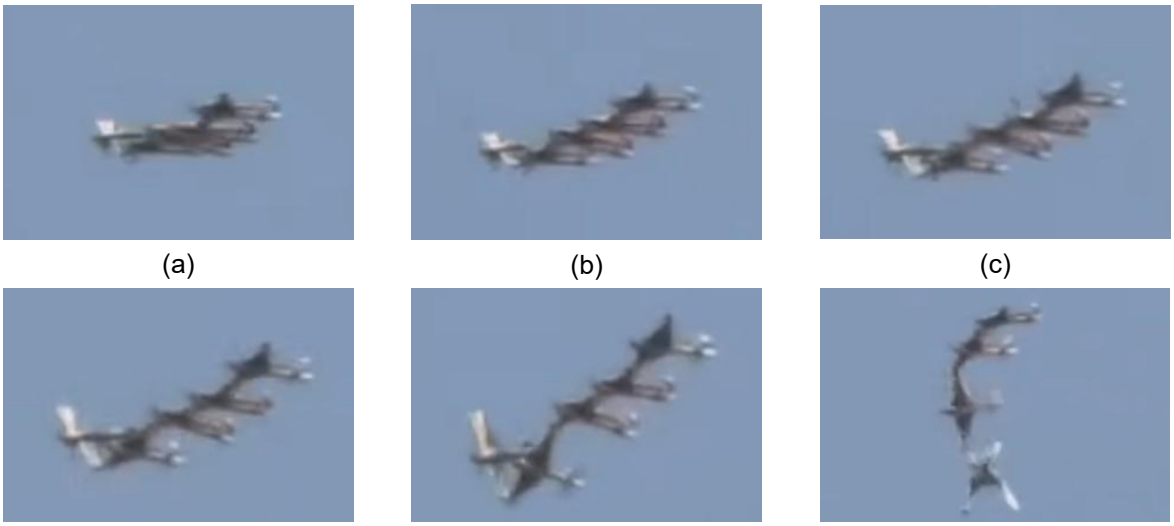


(a) (b)



(c) (d)

Figure 7 - Three-aircraft dihedral divergence instability



(a) (b) (c)

(d) (e) (f)

Figure 8 - Five-aircraft dihedral divergence instability

4.3 Flight Validation with Different Numbers of Units

Stability flight validation is conducted for compound aircraft ranging from single to five units under strong hinge stiffness conditions. The experimental results demonstrate that, in a planar configuration, compound aircraft with various numbers of linked units successfully achieve stable flight. Therefore, the hinge stiffness is a crucial factor affecting the stability of wingtip-linked compound UAVs.



(a) (b) (c) (d)

Figure 9 - Flight tests of two to five aircraft

5. Conclusions

As the number of UAV units in the compound assembly increases, the short period mode frequency and damping ratio show a slight upward trend, the dutch roll mode frequency and damping gradually decrease, and the spiral mode divergence rate slows down. The characteristics of the flapping modes are correlated with the parity of the number of flight units, exhibiting differentiated evolution patterns. When the number of bodies in the compound aircraft is ≥4, non-periodic special motion modes with unclear physical phenomena begin to appear, and the flight dynamics become increasingly complex.

The relative roll angles between the multi-UAVs have a regular impact on modal stability. The short period mode damping ratio improves as the relative roll angle increases, and the stability of the dutch roll mode is simultaneously enhanced. The stability of the spiral mode is closely related to the trim configuration: it is unstable under a dihedral configuration, while its stability significantly improves under an anhedral configuration. The damping coefficient and oscillation frequency of the flapping modes exhibit a significant regular evolution with changes in the relative roll angle.

Hinge stiffness has a weak impact on the conventional rigid-body modes (short period, phugoid, etc.) of the compound multi-body aircraft, but it possesses a significant regulatory effect on flapping modes and special modal characteristics. Increasing the hinge stiffness can transform most flapping modes from real roots to conjugate complex roots, simultaneously enhancing the modal oscillation frequency and damping characteristics.

Although increasing the hinge stiffness can enhance stability, it incurs a greater weight penalty, which contradicts the original intention of utilizing multi-aircraft combinations to improve high-altitude, long-endurance flight performance. Therefore, future research will further analyze the controllability of wingtip-linked compound UAVs, aiming to achieve more agile stable flight and maneuvering flight through stability augmentation control.

6. Contact Author Email Address

mailto: wangrui@nwpu.edu.cn

7. Copyright Statement

The authors confirm that they, and/or their company or organization, hold copyright on all of the original material included in this paper. The authors also confirm that they have obtained permission, from the copyright holder of any third party material included in this paper, to publish it as part of their paper. The authors confirm that they give permission, or have obtained permission from the copyright holder of this paper, for the publication and distribution of this paper as part of the ICAS proceedings or as individual off-prints from the proceedings.

References

[1] McGill S, Schetz J and Mason W. Compound aircraft transport study: Wingtip-docking compared to formation flight. *Proc 41st Aerospace Sciences Meeting and Exhibit*, p 607, 2003.

[2] Montalvo C and Costello M. Meta aircraft flight dynamics. *Journal of Aircraft*, Vol. 52, No. 1, pp 107-115, 2015.

[3] Troub B and Montalvo C J. Meta aircraft controllability. *Proc AIAA Atmospheric Flight Mechanics Conference*, p 3395, 2016.

[4] Montalvo C and Costello M. Meta aircraft connection dynamics. *Proc AIAA Guidance, Navigation, and Control Conference*, p 4677, 2012.

[5] Carithers C and Montalvo C. Experimental control of two connected fixed wing aircraft. *Aerospace*, Vol. 5, No. 4, p 113, 2018.

[6] Cooper J R and Rothhaar P M. Dynamics and control of in-flight wing tip docking. *Journal of Guidance, Control, and Dynamics*, Vol. 41, No. 11, pp 2327-2337, 2018.

[7] Köthe A and Luckner R. Outer-loop control law design with control allocation for a multibody aircraft. *Proc EuroGNC, Milan*, pp 1-20, 2019.

[8] Köthe A and Luckner R. Applying eigenstructure assignment to inner-loop flight control laws for a multibody aircraft. *CEAS Aeronautical Journal*, Vol. 13, No. 1, pp 33-43, 2022.

[9] Köthe A, Behrens A, Hamann A, et al. Closed-loop flight tests with an unmanned experimental multi-body aircraft. *Proc International Forum on Aeroelasticity and Structural Dynamics (IFASD)*, 2017.

[10] Köthe A and Luckner R. Flight path control for a multi-body HALE aircraft. *Advances in Aerospace Guidance, Navigation and Control, Springer, Cham*, pp 421-442, 2018.

[11] An C, Xie C, Meng Y, et al. Flight mechanical analysis and test of unmanned multi-body aircraft. *Proc International Forum on Aeroelasticity and Structural Dynamics (IFASD)*, pp 1-13, 2019.

[12] Köthe A. *Flight mechanics and flight control for a multi-body aircraft*. Ph.D. thesis, Technische Universität Berlin, 2019.

[13] Meng Y, An C, Xie C and Yang C. Conceptual design and flight test of two wingtip-docked multi-body aircraft. *Chinese Journal of Aeronautics*, Vol. 35, No. 12, pp 144-155, 2022.

[14] Zhu E, Zhou Z and Li H. Modal analysis and flight validation of compound multi-body aircraft. *Aerospace*, Vol. 10, No. 5, pp 1-21, 2023.

[15] Fan Y, Bai C, Ren Z, et al. Robust wing shape controller for very flexible aircraft. *Proc Third International Conference on Instrumentation, Measurement, Computer, Communication and Control, IEEE*, pp 1650-1654, 2013.

[16] Lei H, Chen B, Liu Y, et al. Modified Kalman particle swarm optimization: application for trim problem of very flexible aircraft. *Engineering Applications of Artificial Intelligence*, Vol. 100, p 104176, 2021.